Available online at www.sciencedirect.com
ScienceDirect
Geochimica et Cosmochimica Acta 71 (2007) 202–218
Geochimica
www.elsevier.com/locate/gca

Li isotope fractionation in peridotites and mafic melts

A.B. Jeffcoate [a,1], T. Elliott [a,*], S.A. Kasemann [b], D. Ionov [c], K. Cooper [d], R. Brooker [a,e]

[a] *Bristol Isotope Group, Department of Earth Sciences, Wills Memorial Building, Queen's Road, University of Bristol, Bristol BS8 1RJ, UK*
[b] *School of Geosciences, Grant Institute of Earth Science, University of Edinburgh, West Mains Road, Edinburgh EH9 3JW, UK*
[c] *Institut für Mineralogie, J.W. Goethe-Universität, Postfach 111932, 60054 Frankfurt am Main, Germany*
[d] *Geology Department, University of California, Davis, One Shields Avenue, Davis, CA 95616, USA*
[e] *Department of Earth Sciences, University College London, Gower Street, London WC1E 6BT, UK*

Received 15 July 2005; accepted in revised form 5 June 2006

Abstract

We have measured the Li isotope ratios of a range of co-existing phases from peridotites and mafic magmas to investigate high-temperature fractionations of $^{7}Li/^{6}Li$. The Li isotopic compositions of seven mantle peridotites, reconstructed from analyses of mineral separates, show little variation ($\delta^{7}Li$ 3.2–4.9‰) despite a wide range in fertility and radiogenic isotopic compositions. The most fertile samples yield a best estimate of $\delta^{7}Li \sim 3.5‰$ for the upper mantle. Bulk analyses of olivine separates from the xenoliths are typically ~1.5‰ isotopically lighter than co-existing orthopyroxenes, suggestive of a small, high-temperature equilibrium isotope fractionation. On the other hand, bulk analyses of olivine phenocrysts and their host melts are isotopically indistinguishable. Given these observations, equilibrium mantle melting should generate melts with $\delta^{7}Li$ little different from their sources (<0.5‰ lighter). In contrast to olivine and orthopyroxene, that dominate peridotite Li budgets, bulk clinopyroxene analyses are highly variable ($\delta^{7}Li = 6.6‰$ to $-8.1‰$). Phlogopite separated from a modally metasomatised xenolith yielded an extreme $\delta^{7}Li$ of $-18.9‰$. Such large Li isotope variability is indicative of isotopic disequilibrium. This inference is strongly reinforced by *in situ*, secondary ion mass-spectrometry analyses which show Li isotope zonation in peridotite minerals. The simplest zoning patterns show isotopically light rims. This style of zoning is also observed in the phenocrysts of holocrystalline Hawaiian lavas. More dramatically, a single orthopyroxene crystal from a San Carlos xenolith shows a W-shaped Li isotope profile with a 40‰ range in $\delta^{7}Li$, close to the isotope variability seen in all terrestrial whole rock analyses. We attribute Li isotope zonation in mineral phases to diffusive fractionation of Li isotopes, within mineral phases and along melt pathways that pervade xenoliths. Given the high diffusivity of Li, the Li isotope profiles we observe can persist, at most, only a few years at magmatic temperatures. Our results thus highlight the potential of Li isotopes as a high-resolution geospeedometer of the final phases of magmatic activity and cooling.

1. Introduction

The two stable isotopes of Li, ^{6}Li and ^{7}Li, have the biggest relative mass difference of any isotope pair aside from hydrogen and deuterium. This leads to large variability (~50‰) in the isotopic composition of Li in low-temperature, near-surface environments (see review by Tomascak, 2004) dominantly resulting from exchange reactions of clays with fluids (Chan et al., 1992; Zhang et al., 1998; Huh et al., 2001; Pistiner and Henderson, 2003). The transport, via subduction, of such fractionated material to the mantle should impart distinctive isotopic signatures and so Li isotope measurements are potentially a powerful tracer of 'recycled' crustal material in the mantle (see Elliott et al., 2004). The large relative mass difference in the Li isotopic system, however, may also lead to significant high-temperature isotopic fractionations and these need to be assessed if Li isotopes are to be used as a fingerprint of recycling. Systematic fractionations of the stable isotopes of several major elements have been observed between mantle mineral phases, see Fig. 1. Seitz et al. (2004) and

* Corresponding author. Fax: +44 117 925 3385.
E-mail address: tim.elliott@bris.ac.uk (T. Elliott).
[1] Present address: Rio Tinto Iron Ore Atlantic Ltd, P.O. Box 695, 8th Floor, Castlemead, Lower Castle Street, Bristol BS99 1FS, UK.

0016-7037/$ - see front matter © 2006 Elsevier Inc. All rights reserved.
doi:10.1016/j.gca.2006.06.1611

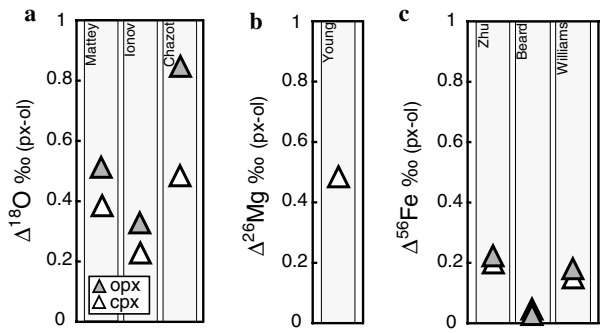

Fig. 1. Stable isotope fractionations between the mantle phases olivine, clinopyroxene, and orthopyroxene for several isotope systems reported in the literature. Fractionations between pyroxenes and olivine (Δ_{px-ol}) are shown as the differences between their isotope ratios (expressed as parts per thousand differences relative to a standard, i.e., δ values). The isotope ratios and standards used to derive the Δ values are (a) $^{18}O/^{16}O$ relative to standard mean ocean water (SMOW), (b) $^{26}Mg/^{24}Mg$ relative to NBS980 and (c) $^{56}Fe/^{54}Fe$ relative to IRMM-014. Where several analyses of inter-mineral fractionation were presented, the values of Δ were averaged. Sources for the data are Mattey et al. (1994), Ionov et al. (1994), Chazot et al. (1997), Young et al. (2002), Zhu et al. (2002), Beard and Johnson (2004) and Williams et al. (2005). In (a) we focus on high-precision laser-fluorination oxygen isotope data but see Kyser (1986) for summary of earlier work by conventional fluorination techniques. We do, however, report analyses obtained using conventional fluorination for the Vitim xenolith suite (Ionov et al., 1994), for which there was a careful inter-comparison between conventional and laser assisted fluorination methodologies.

most recently Magna et al. (2006) have reported significant Li isotope variability between co-existing mantle phases, which they attribute to equilibrium, inter-mineral fractionations. These measurements imply that mantle-derived melts, the primary sample of the Earth's interior, may not have the same Li isotope compositions as their sources.

Tomascak et al. (1999) showed that there are no systematic variations in Li isotope ratios within a suite of cogenetic Hawaiian lavas related by mineral fractionation and accumulation. This placed an important constraint on the magnitude of Li isotope fractionation during magmatic differentiation. The work of Tomascak et al. (1999) does not provide sufficient information, however, on specific melt–mineral fractionations to predict the isotopic composition of a primitive mantle melt relative to its source. Chan and Frey (2003) have further reported analyses of olivine and matrix pairs from several Hawaiian samples which show the same δ^7Li, within analytical reproducibility. Here, we explore in greater depth high-temperature Li isotope fractionations using a wider range of volcanic phenocryst–matrix pairs and co-existing phases separated from mantle xenoliths, employing both bulk, multi-collector inductively coupled plasma mass-spectrometry (MC-ICP-MS) and *in situ* secondary ionisation mass-spectrometry (SIMS) analyses. We also consider the influence of diffusive fractionation, which several recent studies have shown to be effective in generating Li isotopic variability at magmatic temperatures (Richter et al., 2003; Lundstrom et al., 2005; Teng et al., 2006).

2. Samples

Melt–olivine fractionation was assessed by looking at a holocrystalline lava with large (~1 mm) olivine phenocrysts (Th29) and a glassy sample with smaller (~0.5 mm) phenocrysts (AH). Th29 is a post-glacial (<8000 y) picritic flow from Theistareykir, Iceland (Elliott et al., 1991). AH is a basaltic glass collected by the first author from the quenched margin of the 1997 Pu'u O'o flow, Kilauea, Hawaii, USA (Heliker et al., 1998). Table 1 provides compositional information on these samples.

In order to study possible isotopic fractionations between a wider range of phenocrysts we also examined two well-studied Hawaiian flows, 97KC05 and 97KC06 (Cooper et al., 2001), that contained co-existing olivine, plagioclase and clinopyroxene. 97KC05 represents the early phase of Kilauea's, 1955 east rift eruption. It is a relatively evolved lava with ~5.5 wt% MgO (Wright and Fiske, 1971) which contains well-developed crystals of clinopyroxene and plagioclase together with minor olivine. The other sample, 97KC06, is from the 1960 vents (Wright and Helz, 1996). It has large olivine and clinopyroxene crystals as well as smaller, resorbed plagioclases. The petrography of 97KC06 is typical of the late 1960 flows and is indicative of mixing a primitive olivine bearing magma with a more evolved residue from the 1955 event (Wright and Helz, 1996). In addition to bulk mineral separate analyses, we studied two phenocrysts from 97KC06 in some detail by SIMS, a normally zoned olivine and a reversely zoned pyroxene (Table 1).

We also analysed co-existing mineral phases separated from seven mantle xenoliths (Table 2). All the xenoliths were hosted by alkali basalts and represent off-craton continental lithospheric mantle (CLM). The majority of xenoliths in this study are from the Central Asian orogenic belt that lies between the Siberian and North China cratons. Our samples come from three localities within this region, namely Vitim in southern Siberia (Ionov, 2004; Ionov et al., 2005a) and the Tariat Depression and Dariganga plateau in Mongolia (Ionov and Wood, 1992). We have analysed both garnet and spinel peridotites with mineral equilibrium temperatures ranging from ~870 to 1150 °C and pressures up to ~23 kbar (Ionov, 2004; Ionov et al., 2005a). These xenoliths are texturally equilibrated rocks, with no optical zoning. The samples appear to be in chemical equilibrium, aside from some major element zoning in the rims of pyroxenes from garnet peridotites, as well as breakdown of garnet rims to form kelyphite, which reflects heating shortly before eruption (Ionov, 2004; Ionov et al., 2005a). We also investigated one sample (SC) from the San Carlos volcanic field in the southwestern United States. Xenoliths from this locality have been extensively studied mineralogically, chemically and isotopically (Frey and Prinz, 1978; Zindler and Jagoutz, 1988; Galer and O'Nions, 1998). Our SC sample has a granular texture with large (1–5 mm) olivine and orthopyroxene grains but small (0.1–1 mm) and sparse (<5%) clinopyroxene crystals.

Table 1
Major element compositions (in weight percent) of the volcanic samples and associated phenocrysts used in this study

	Th29 wr	AH gl	Kilauea 1960 gl	Kilaeua 1955 gl	Th29 ol	AH ol core	AH ol rim	97KC06 ol core	97KC06 ol rim	97KC06 cpx core	97KC06 cpx rim
SiO_2	*47.5*	51.8	*50.6*	*51.3*	40.5	39.1	38.6	40.1	38.7	50.5	51.5
TiO_2	*0.5*	2.48	*3.01*	*3.5*						1.26	0.88
$A1_2O_3$	*13.4*	13.5	*13.9*	*13.8*						2.7	2.2
FeO^T	*8.2*	10.8	*10.9*	*12.2*	9.9	16.1	17.4	12.8	19.8	9.5	7.9
MnO	*0.2*	0.2	*0.2*	*0.2*	0.2	0.2	0.3	0.2	0.2	0.3	0.2
MgO	*15.7*	6.5	*6.5*	*5.5*	48.5	43.8	42.8	45.9	40.1	16.5	16.6
CaO	*12.5*	10.9	*10.8*	*9.4*	0.4	0.3	0.3	0.3	0.3	17.5	18.8
Na_2O	*1.1*	2.3	*2.7*	*2.8*						0.26	0.26
K_2O	*0.01*	0.31	*0.65*	*0.74*							
P_2O_5	*0.02*	0.25	*0.28*	*0.4*							
NiO					0.35	0.27	0.21	0.40	0.28		
Total	*99.1*	99.1	*99.6*	*99.8*	99.8	99.8	99.6	99.7	99.4	98.4	98.3
Mg#	*0.80*	0.56	*0.56*	*0.48*	0.90	0.83	0.81	0.87	0.78	0.76	0.79

Analyses were largely performed using the JEOL 8600 electron microprobe at the University of Bristol using standard operating conditions of 20 kV accelerating voltage and 15 nA beam current. Matrix corrections were made using the ϕ–ρ–z approach. Calibrations were made using a range of silicate and natural glass standards including St. John's Island olivine and BCR-1G basaltic glass standard. For some samples, data already available in the literature are reported here for easy reference (in italics). The whole rock Th29 analysis is taken from Elliott et al. (1991). Glass compositions reported for 1960 and 1955 Kilauea flows are for samples comparable to our KC97 06 and KC97 05, taken from Wright and Helz (1996) and Wright and Fiske (1971). Abbreviations: Mg# = molar Mg/[Fe(II) + Mg] × 100, assuming here that Fe(II)/Fe(total) = 0.85 for whole rocks and glasses; wr, whole rock; gl, glass; ol, olivine; cpx, clinopyroxene.

Table 2
Background information for xenolith samples

Sample	Location	Rock type	Age (Ma)	T (°C)	P (kbar)	Mineral modes (%)						WR		Ol Fo%	Cpx	
						Ol	Opx	Cpx	Spl	Gnt	Phl	MgO wt%	CaO wt%		$(La/Sm)_N$	ε_{Nd}
313-105	Vitim	Gnt. Lh.	16	1034	21.3	63	17	12		8.3		40.4	2.9	89.9		14.0
313-102	Vitim	Gnt. Lh.	16	1053	22.9	50	23	14		14		36.7	3.4	89.3	0.66	
314-56	Vitim	Spl. Lh.	16	889	<18	51	30	17	2.5			37.2	3.5	88.6	0.39	14.6
Mo-Z-1	Tariat	Spl. Lh.	0.52	890	<18	55	21	20	2.4			38.1	4.0	*89.3*	0.57	
4230-16	Tariat	Spl. Phl. Lh.	0.5	867	<18	56	22	19	3.1		0.6	37.0	3.8	*89.6*	1.43	2.2
8505-2	Dariganga	Spl. Hz.	1–20	914	<18	76	20	2.8	1.1			48.6	0.8	90.8	2.1	3.9
SC	San Carlos	Spl. Lh.	~0.6	*1002*	<18	62	32	5.6	0.5			*43.3*	*1.4*	89.8	*0.9*	*6.8*

Reference data taken from Ionov et al. (1993), Ionov (2004), Ionov et al. (2005b), Stosch et al. (1986) and Press et al. (1986). Olivine compositions were measured as part of this study (see Table 1 caption for details on electron probe measurements) except for 4230-16 and Mo-Z-1, for which literature data are reported in italics. Data for the sample SC (collected by R.B.) come from our own point counting (500 points) and electron probe analysis, from which we have inferred other data (shown in italics) using compositional co-variations for a larger suite of San Carlos xenoliths reported in Frey and Prinz (1978) and Galer and O'Nions (1998). Abbreviations as in caption to Table 1 and additionally: opx, orthopyroxene; spl, spinel; gnt, garnet; phl, phlogopite, lh, lherzolite; hz, harzburgite.

The selection of xenoliths encompasses nearly the complete spectrum of modal and major element compositions shown by off-craton peridotites, from very fertile, near-primitive (e.g., 4.0% CaO, Mo-Z-1) to highly refractory (0.8% CaO, 8505-2), see Table 2. We have concentrated, however, on the more fertile, anhydrous central Asian xenoliths, which represent a suitable source for typical mantle melts. These xenoliths are also some of the least disturbed CLM samples worldwide, in terms of their incompatible element compositions, as shown by clean clinopyroxene separates with chondrite normalised La/Sm <1 and high ε_{Nd} (Ionov, 2004; Ionov et al., 2005a), see Table 2. These samples are thus chemically and isotopically similar to source regions of mid-ocean-ridge basalts (MORB). As a contrast, we also analysed modally metasomatised sample 4230-16, which contains phlogopite and a cryptically metasomatised harzburgite, 8505-2. Both of these samples have clinopyroxenes with chondrite normalised La/Sm >1 (Table 2). The San Carlos xenolith suite has also been cryptically metasomatised (Frey and Prinz, 1978), with the effects of metasomatism most evident in the trace element chemistry of samples that experienced the greatest prior melt extraction. We have studied a depleted San Carlos peridotite with ~5% clinopyroxene. By comparison to literature data, this sample should be significantly influenced by cryptic metasomatism, although we

have not determined its trace element nor radiogenic isotopic compositions.

3. Sample preparation and analytical procedures

3.1. Mineral separation

Samples were initially crushed and sieved to allow a rough separation of appropriate phases. A secondary crushing procedure further reduced grain size to allow a subsequent, stringent picking of ~10 mg of only the cleanest, alteration-, crack- and discolouration-free fragments. This preparation process likely preferentially removes the outer portions of minerals. Moreover, all peridotite separates, with the exception of SC, underwent lengthy and powerful, ultra-sonic disaggregation during their original preparation in Moscow. This procedure was originally undertaken to ensure pure clinopyroxene separates, but the unusually aggressive treatment should also have efficiently removed the outer portions of all minerals and any interstitial glass. Finally, separates were washed in high-purity 18 MΩ cm water (Milli-Q). One set of SC separates was further ultra-sonically washed for 15 min in Milli-Q water (Table 3). Some of the central Asian orthopyroxenes and clinopyroxenes had also previously been leached in 6 N HCl (see Table 3) and are splits of separates already analysed for trace elements and Sr–Nd–Hf isotopes (Ionov, 2004; Ionov et al., 2005a). The purified samples were dissolved and their Li fractions separated according to the procedure of Jeffcoate et al. (2004).

3.2. Bulk analysis by MC-ICP-MS

Li isotope ratios and Li concentrations were measured on the Thermo Finnigan Neptune MC-ICP-MS, at Bristol University. Most of the Li sample solutions were analysed in duplicate. δ^7Li values were measured by a rapid standard-sample-standard bracketing technique, using the certified reference material NIST L-SVEC. The reproducibility of the Li isotope ratios of homogeneous international rocks standards is <0.3‰ ($2\sigma_{sd} = 2$ standard deviations), and repeatability of the same sample solution is <0.2‰ $2\sigma_{sd}$. Jeffcoate et al. (2004) provide a more detailed description of the analytical procedure.

The reproducibility of mineral separate measurements was assessed by repeating the entire picking and dissolution procedure for certain xenoliths (Table 3). Full duplicate analyses were made for olivine, orthopyroxene and clinopyroxene from samples 313-105 and SC. The results of the repeat measurements for 313-105 were well within our previously determined analytical uncertainty of ±0.3‰, but slightly larger variability was evident in repeat measurements of SC. Given the large degree of heterogeneity documented within individual mineral grains by SIMS (see below) it is not surprising that the reproducibility for this sample is anomalously poor. Indeed, the relatively modest variability of full SC repeats illustrates the effective averaging of isotopic heterogeneity achieved by analyses of bulk separates. We also assessed the influence of ultrasonic cleaning of mineral separates, which Seitz et al. (2004) suggested was critical. Twenty milligrams of hand-picked SC olivine, orthopyroxene and clinopyroxene separates were split into two sets of ~10 mg samples, with one washed only by manual agitation in Milli-Q water and the other ultrasonified in Milli-Q water for 15 min. We

Table 3
Summary of the Li isotope ratio and concentration data measured by MC-ICP-MS

Sample	Description	Mineral	δ^7Li	2σ	[Li] (ppm)	2σ	Bulk δ^7Li
313-105	Gnt Lh	Ol	4.7	0.2	2.32	0.09	4.3
		Opx*	3.4	0.2	1.5	0.10	
		Cpx	1.1	0.3	1.12	0.08	
		Gnt	2.7	0.2	0.12	0.002	
313-105 (rep)	Gnt Lh	Ol	4.9	0.3	2.4	0.10	
		Opx	3.4	0.2	1.60	0.10	
		Cpx	1.0	0.2	1.18	0.08	
313-102	Gnt Lh	Ol	3.7	0.2	1.97	0.09	3.7
		Opx	3.5	0.2	1.00	0.14	
		Cpx	3.5	0.2	1.15	0.08	
		Gnt	4.4	0.1	0.15	0.002	
314-56	Spl Lh.	Ol	3.0	0.2	1.87	0.09	3.9
		Opx	4.4	0.1	1.37	0.10	
		Cpx	6.6	0.2	1.30	0.09	
Mo-Z-1	Spl Lh	Ol	3.0	0.1	1.93	0.08	3.2
		Opx	4.5	0.2	1.25	0.10	
		Cpx	2.6	0.2	1.11	0.07	
4230-16	Spl Phl Lh	Ol	3.1	0.2	1.75	0.08	
		Cpx*	4.7	0.2	1.15	0.09	
		Phl*	−18.9	0.1	0.85	0.19	
8505-2	Spl Hz	Ol	3.0	0.2	1.40	0.09	3.3
		Opx*	4.6	0.1	1.25	0.08	
		Cpx*	1.6	0.2	1.25	0.09	
SC no ultra-sound	Spl Lh	Ol	5.2	0.2	2.38	0.10	4.9
		Opx	6.4	0.2	1.17	0.09	
		Cpx	−7.8	0.1	1.48	0.07	
SC (rep) no ultra-sound	Spl Lh	Ol	4.8	0.1	2.31	0.12	4.5
		Opx	6.1	0.2	1.15	0.10	
		Cpx	−8.7	0.1	1.50	0.04	
SC (rep) with ultra-sound	Spl Lh	Ol	5.0	0.2	2.29	0.09	4.8
		Opx	6.7	0.1	1.20	0.05	
		Cpx	−8.1	0.2	1.48	0.02	
Th29	Icelandic Basalt	Ol	3.3	0.2	1.25	0.10	
		Matrix	3.4	0.2	4.50	0.12	
AH	Hawaiian Basalt	Ol	3.5	0.07	1.42	0.12	
		Gl	3.7	0.04	3.22	0.13	
97KC06 (1960)	Hawaiian Basalt	Ol	6.6	0.60	1.18	0.12	
		Cpx	1.6	0.17	0.85	0.15	
		Plag	−2.6	0.19	1.55	0.11	
97KC05 (1955)	Hawaiian Basalt	Ol	6.5	0.14	1.28	0.12	
		Cpx	1.8	0.24	0.78	0.20	
		Plag	2.0	0.25	1.75	0.10	

Clinopyroxenes and orthopyroxenes acid-leached before analysis are indicated with an asterisk. Bulk reconstructed δ^7Li calculated using modal analyses in Table 2. Reported errors are 2 sigma standard deviations of repeat measurements of the same sample dissolution.

found no obvious effect of the ultra-sonic treatment on Li isotope ratios (Table 3). Likewise acid-leached and non-acid-leached orthopyroxenes, admittedly from different samples, show no systematic differences which suggests that this procedure little influenced measured Li isotope ratios (Table 3).

3.3. In situ analysis by SIMS

Resin mounts of glass fragments from Hawaiian sample AH, thin sections of Hawaiian flows 97KC05 and 97KC06, resin mounts of large olivine and orthopyroxene separates from 314-56 and picked mineral clusters from SC were polished, cleaned and gold coated for secondary ionisation mass-spectrometry (SIMS) analysis.

The SIMS analyses were carried out on the single-collector Cameca ims 4f at the NERC Ion Microprobe Facility at the University of Edinburgh. Positive secondary ions ($^6Li^+$, $^7Li^+$) were produced by a $^{16}O^-$ 30 nA primary beam focused to a 30 μm spot size with a net impact energy of 14.5 keV. The secondary ions were analysed with an energy window of 52 eV, a 150 μm image field using the 150 μm contrast and the 1800 μm field apertures. In order to obtain better counting statistics, we later used a more intense primary beam (40 nA) with 400 μm contrast aperture. This increased ion count rates about 50% without changing the value obtained for the BCR standard. These operating conditions were only used, however, for a single set of data presented in this study (Fig. 8a). Analyses were made using a mass resolution of ~1200, which enabled resolution of $^6LiH^+$ from $^7Li^+$ and $^{12}C^{2+}$ from $^6Li^+$. The Li isotope ratios were measured for 100 cycles on the electron multiplier, each cycle consisting of 5- and 2-s count times on $^6Li^+$ and $^7Li^+$, respectively. Further details can be found in Kasemann et al. (2005). The "internal" uncertainties $2\sigma_{se}$ ($2\sigma_{se} = 2$ standard errors) of individual measurements typically range from about ±1‰ for high Li concentration (~5 μg g^{-1}) natural glasses to ±4.5‰ in clinopyroxenes with Li concentrations as low as 0.7 μg g^{-1}.

The SIMS data are reported in the conventional δ^7Li notation relative to L-SVEC. Calibration to the international reference material was through the USGS reference glass BCR-2G using a δ^7Li value of 4.1‰, as independently measured by MC-ICP-MS with respect to L-SVEC (see Kasemann et al., 2005). We further checked accuracy by measurement of GSD-1G. SIMS analyses of BCR-2G showed an internal uncertainty of 0.6–1‰ ($2\sigma_{se}$) for a single point analysis and a 1-day external uncertainty of 1-2‰ ($2\sigma_{sd}$). For our 5-day analytical session, in which the data presented here were largely collected, the external reproducibility was ~3‰ ($2\sigma_{sd}$). This reproducibility is slightly worse than is typical (cf. Kasemann et al., 2005) which we attribute to an ageing electron multipler.

Kasemann et al. (2005) obtained Li isotopic data by MC-ICP-MS, TIMS and SIMS on a variety of natural and synthetic reference glasses to investigate the influence of varying major element matrices. They found no discernable matrix dependence on the SIMS measurements for all the natural and USGS synthetic glass samples. We have similarly assumed that there is no systematic instrumental mass bias between melt and different mineral phases (after Decitre et al., 2002). As we discuss in Section 5.1, however, there is evidence that this may not always be the case but in the absence of sufficiently detailed calibrations, we feel it most straightforward to make no corrections.

In situ lithium concentrations were measured by SIMS using a peak jumping routine between ^7Li and ^{30}Si, with 5- and 2-s integrations, respectively. A full analysis comprised 40 cycles. Typical ^7Li count rates for olivines were ~250 cps, yielding uncertainties of <1% ($2\sigma_{se}$) for an analysis. Measured Li/Si ratios were normalised to NIST SRM 610 reference material using the recommended values from Pearce et al. (1997). Li concentrations were finally calculated from the Li/Si ratio determined by SIMS in combination with the Si content of the analysed phase as measured independently by electron probe. The long-term reproducibility of Li concentration determinations is typically ⩽10% ($2\sigma_{sd}$), but within an individual analytical session the difference in concentration between adjacent points in a single phase can be determined to ~1% (counting statistics permitting). Values for internationally available glass standards measured by this technique are reported in Kasemann et al. (2005). As with SIMS isotope ratio measurements, instrumental mass-fractionation is assumed to be the same for all phases.

4. Results

4.1. MC-ICP-MS

MC-ICP-MS isotope data are reported in Table 3 and displayed in Fig. 2. The δ^7Li of olivine phenocrysts and their host glass or matrix are within our analytical uncertainty (±0.3‰). The 97KC06 and 97KC05 Hawaiian samples were used to assess inter-mineral fractionations (the possibly slightly altered groundmass was not analysed). For both samples the olivines have similar compositions and are ~5‰ heavier than co-existing clinopyroxenes (Fig. 2a). The plagioclases are isotopically light but do not show a consistent offset with respect to the other minerals.

The Li isotopic compositions of minerals separated from the mantle xenoliths show significant variations (Fig. 2b). Yet olivines, the principal hosts of Li in the mantle, show a rather limited range in Li isotope composition from $\delta^7Li = 3.0$ to 5.2‰. Similarly, orthopyroxene analyses vary by only ~3‰. In all five spinel facies xenoliths the orthopyroxene is heavier than the olivine by ~1.5‰. However, no systematic fractionation is observed between olivine and clinopyroxene. Clinopyroxene shows a much greater variability in isotopic composition than the other phases, ranging from $\delta^7Li = 6.6$ to −8.7‰. In the fertile peridotites, clinopyroxenes typically have δ^7Li heavier than co-existing olivines, whereas in more depleted samples the clinopyroxenes tend to be lighter (Fig. 3a).

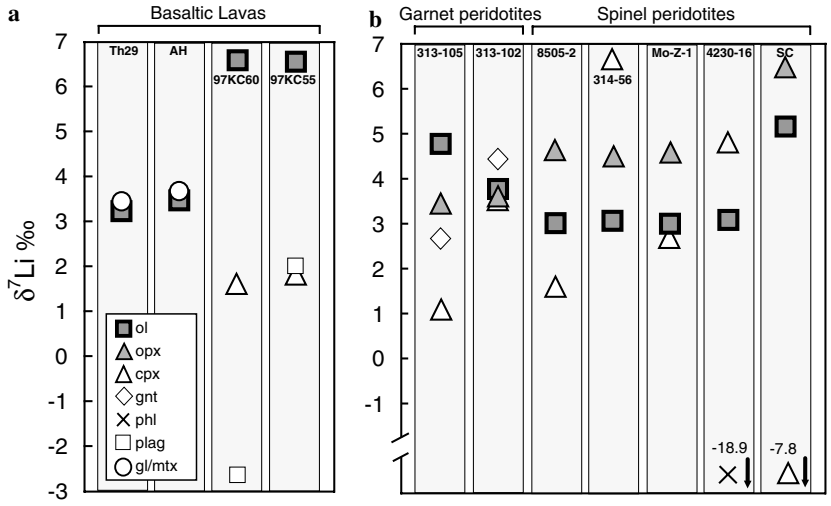

Fig. 2. MC-ICP-MS data for (a) lavas and phenocrysts and (b) xenolith mineral separates. Abbreviations as given in caption to Tables 1 and 2 and additionally matrix = mtx, plag = plagioclase.

Spinels were not analysed due to difficulty in their dissolution. Spinels contain very little Li (Seitz and Woodland, 2000) and so have a negligible influence on the bulk δ^7Li of the xenoliths. The Li concentrations of our garnet separates are low, ~0.15 μg g^{-1}, indicating the higher-pressure aluminous phase is also insignificant in the Li isotopic budget of the mantle. Metasomatic phlogopite (in sample 4230-16) has a very light Li isotopic signature ($\delta^7Li = -18.9‰$) but only a modest Li abundance (0.85 μg g^{-1}).

The higher abundances of Li in olivine relative to clinopyroxene (and orthopyroxene) in our fertile xenoliths (Fig. 3b) are in keeping with equilibrium partitioning as inferred by Seitz and Woodland (2000). Likewise, the Li abundances in our olivines are generally consistent with a trend of melt extraction suggested by Seitz et al. (2004), although two of our samples have Li-enriched olivines compared to their model melt residue curve (Fig. 3b). In the most refractory sample (8505-2), the difference in the Li concentrations between olivine and clinopyroxene is much reduced. This is a characteristic Seitz and Woodland (2000) have previously attributed to metasomatic enrichment of Li in the clinopyroxene.

Bulk xenolith δ^7Li values were calculated using modal abundances (Table 2, ignoring spinel) together with mineral Li isotope and abundance data (Table 3). Such reconstructed bulk compositions from this study and Seitz et al. (2004) are shown in Fig. 3c together with bulk analyses of a single San Carlos xenolith (Seitz et al., 2004) and other Dariganga xenoliths (Magna et al., 2006). It is notable that the measured δ^7Li of the San Carlos bulk xenolith is 2.5‰ lighter than the composition calculated from its constituent minerals. The reconstructed bulk compositions of our fertile xenoliths fall within the range of high-precision N-MORB measurements, δ^7Li ~3–4‰ (Elliott et al., 2004).

4.2. SIMS

All SIMS data are documented in electronic annex EA-1 and are presented in Figs. 4–10.

4.2.1. Hawaiian samples

The average composition of the Hawaiian sample (AH) measured by SIMS ($\delta^7Li = 4.4 \pm 0.8‰$, $2\sigma_{se}$) compares well with the more precise bulk MC-ICP-MS analysis of 3.7‰ (Fig. 4 and Table 3). Olivines from AH show no discernible Li isotope zonation (Fig. 5 and EA-1) but have a mean ($5.7 \pm 0.7‰$, $2\sigma_{se}$) heavier than the bulk MC-ICP-MS measurement (3.5‰). The microphenocrysts of clinopyroxene and plagioclase in AH have Li isotopic compositions that range to values as light as $\delta^7Li = -7.5‰$ and −8‰ at their rims (see Fig. 4 and EA-1).

Mineral phases in the holocrystalline 97KC05 and 97KC06 Hawaiian lavas show significant Li isotope zonation. Fig. 6a shows a profile across a 600 μm diameter clinopyroxene from 97KC06, with δ^7Li ranging from −9.8 to 13.7‰. Li concentrations also show zoning in this grain, with values of 2.7 μg g^{-1} at the rim to around ~0.8 μg g^{-1} in core. The isotopic variations appear to extend further into the body of the crystal than the changes in Li abundance. A similar pattern of isotopic and elemental zonation is observed in a 1000 μm olivine from the same sample (Fig. 6b). The magnitude of zoning in the olivine is smaller, from $\delta^7Li = 6.9‰$ in the core to −2‰ at the rim. Fig. 7 shows histograms of SIMS analyses of mineral phases from the 97KC05 and 97KC06 Hawaiian basalts, combining the analyses of zoned minerals shown in Fig. 6 with a larger number of additional grains represented by only single spot analyses. A wide range of clinopyroxene compositions is evident, with values both heavier and lighter than co-existing olivines (Fig. 7). The few plagioclase measurements show much lighter δ^7Li in the 97KC06 relative to the

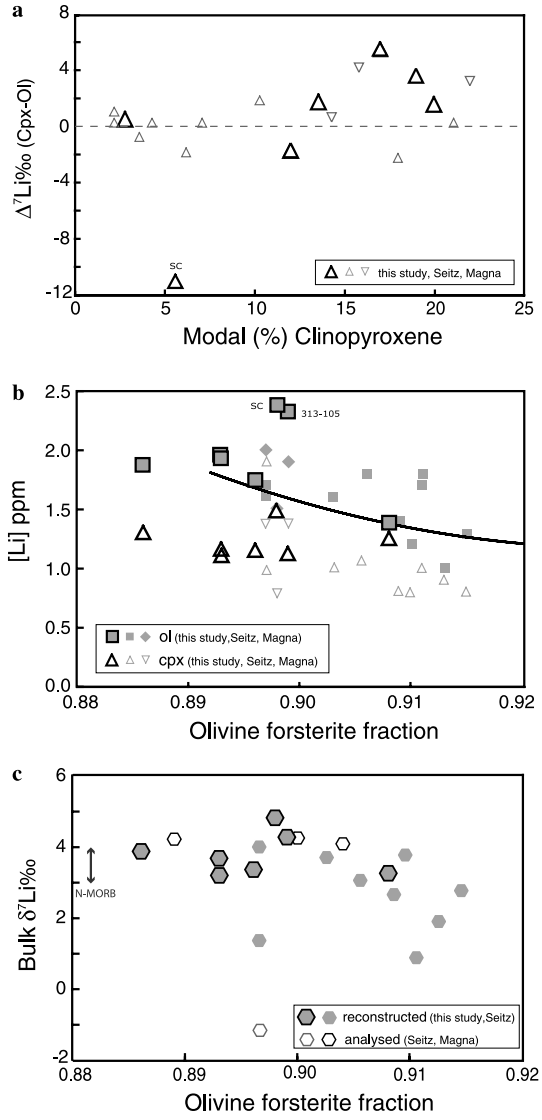

Fig. 3. (a) Modal clinopyroxene abundance in each xenolith plotted against δ^7Li of separated clinopyroxene measured by MC-ICP-MS. Literature data (Magna et al., 2006; Seitz et al., 2004) reported for comparison in smaller symbols. (b) Li concentrations ($\mu g\ g^{-1}$) of olivines (filled squares) and clinopyroxene (open diamonds) plotted against the forsterite content (mole fraction) of olivines in the same xenolith. Olivines and clinopyroxenes from Seitz et al. (2004) and Magna et al. (2006) are again shown for reference as smaller symbols. The line indicates changing olivine compositions in response to melt depletion, after Seitz et al. (2004). This melt depletion reference curve is calculated using the mineral and melt modes from the melting experiments of Hirose and Kushiro (1993) assuming [Li] of 2.0 $\mu g\ g^{-1}$ and D_{Li} of 0.35. (c) Reconstructed bulk δ^7Li values for xenoliths (see text for details) from our study and from Seitz et al. (2004) plotted against the forsterite content (mole fraction) of olivines in the xenolith. The absence of both orthopyroxene and clinopyroxene analyses in the peridotites measured by Magna et al. (2006) mean that these samples cannot be properly plotted on this diagram, but their olivine compositions (δ^7Li ~ 3.5‰), which dominate the bulk composition, are similar to ours. Also plotted is a single bulk xenolith analysis (open hexagon) from Seitz et al. (2004) and the corresponding the reconstructed bulk value of the same xenolith lies directly above it. Further analyses of bulk xenoliths, from the Dariganga plateau near our sample 8505, from Magna et al. (2006) are plotted as open hexagons with darker rims. The range of N-MORB δ^7Li from Elliott et al. (2004) is indicated for reference.

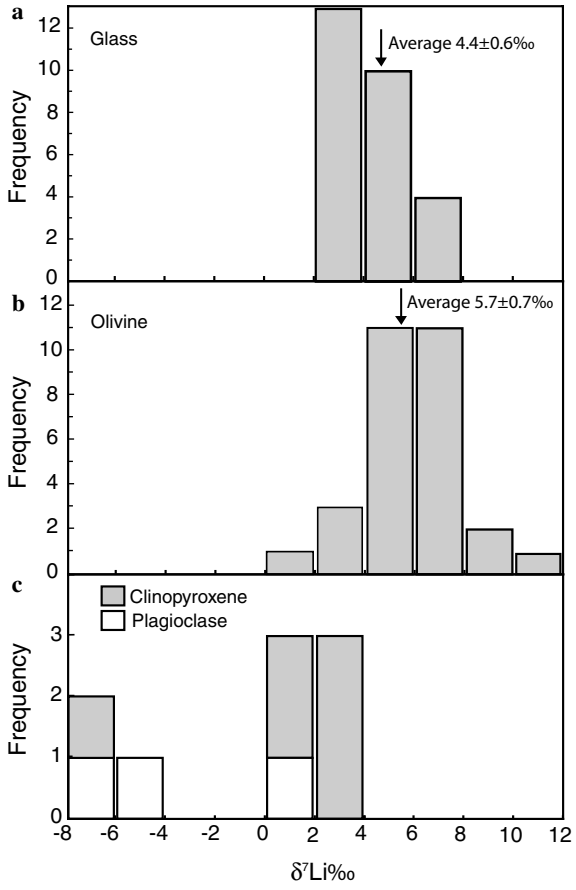

Fig. 4. Histograms of SIMS analyses of different phases in AH Hawaiian basalt sample, (a) glass, (b) olivine and (c) clinopyroxene and plagioclase.

97KC05 lava (Fig. 7b and c), in keeping with the bulk analyses by MC-ICP-MS (Fig. 2a) although at markedly different absolute values.

4.2.2. Xenoliths

As with phenocrysts in the holocrystalline Hawaiian samples, large Li isotopic variations are observed within individual mineral grains of the xenoliths.

A large (~1 mm diameter) olivine fragment from 314-56 shows δ^7Li that varies from 6‰ at the core to −2‰ at the rim (Fig. 8a). A perpendicular traverse made using a more intense primary beam, to obtain higher precision, confirms this pattern of zoning (Fig. 8b). An orthopyroxene from the same sample shows a similar style of zonation (Fig. 8c). In both grains, higher Li abundances in the rims are associated with much lower δ^7Li (Fig. 8). We note that the δ^7Li values measured in the grain cores by SIMS are similar to those obtained by MC-ICP-MS in the bulk mineral separates of this sample.

In order to analyse material retaining original grain boundaries, we also examined chunks of material from the SC xenolith (Figs. 9 and 10). A detailed Li isotope transect of an olivine from this sample (Fig. 9a) showed large variations but with an opposite sense of zonation to the minerals from xenolith 314-56 (Fig. 9b). The SC olivine becomes progressively heavier away from a light core (δ^7Li −5‰) to

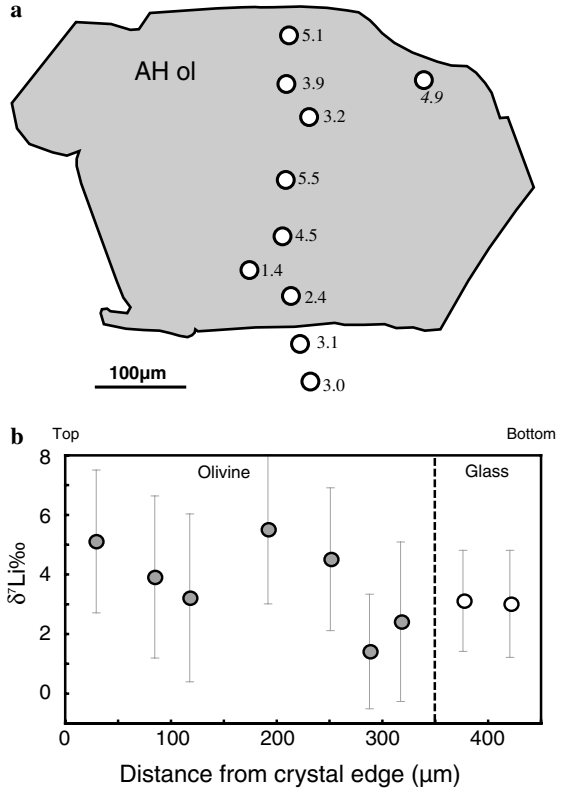

Fig. 5. (a) Trace outline of AH olivine (grey) within surrounding glass, showing the position of the Li isotopic measurements by SIMS. (b) Plot of measured δ^7Li values (with $2\sigma_{se}$ errors) against distance across traverse.

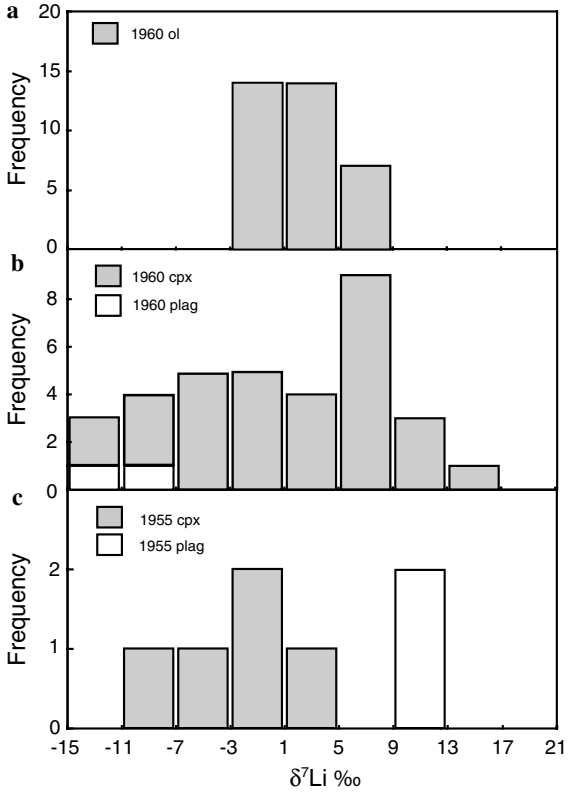

Fig. 7. Histograms of SIMS Li isotope measurements of the various phenocrysts in (a and b) 97KC06, 1960 Hawaii flow and (c) 97KC05, 1955 Hawaii flow.

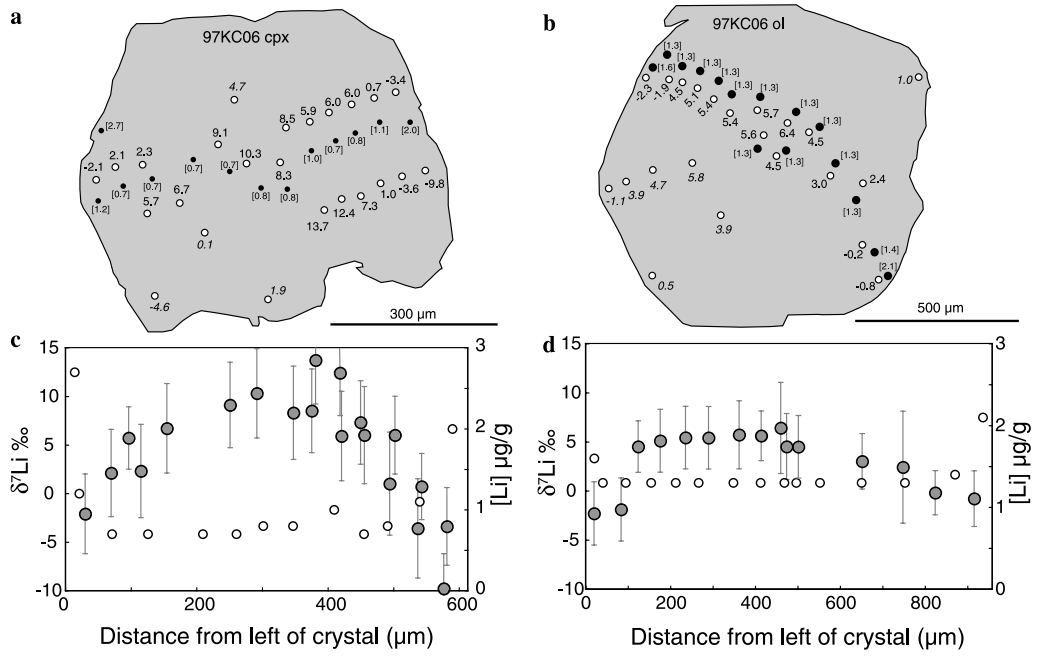

Fig. 6. Trace outlines of (a) clinopyroxene and (b) olivine phenocrysts from 1960 Hawaii flow 97KC06 within surrounding matrix to show the position of the Li isotopic and [Li] measurements (μg g^{-1}) by SIMS. (c) and (d) are corresponding plots of Li isotope (filled circles) and concentration (open circles) from (a) and (b), respectively, that form a single profile across the crystals. The position of data points were calculated as a distance from the edge of the crystal. Points off the main line of the traverse are not plotted and shown on (a) and (b) in italics, although this makes little difference to the plots. $2\sigma_{se}$ error bars for the isotope ratio measurements are shown. Nominal uncertainties for the Li concentrations are ± 0.1 μg g^{-1} $2\sigma_{sd}$, but in practice the repeatability of the olivine core concentrations within a traverse appears better than this.

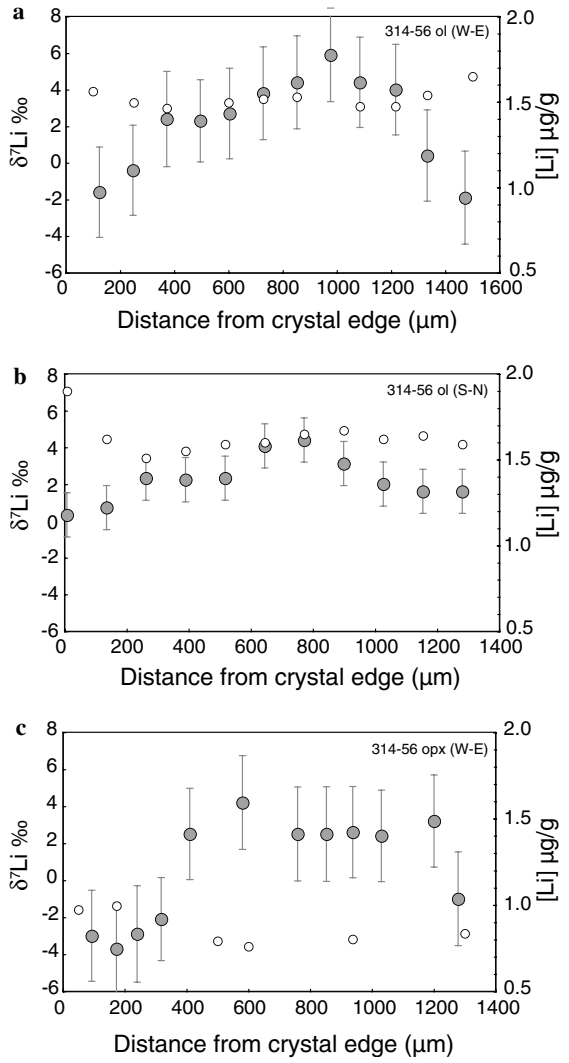

Fig. 8. SIMS Li isotope (filled circles) and concentration (open circles) data for traverses of mineral separates from 314-56. (a) and (b) perpendicular traverses of an olivine crystal. The profile in (b) was made using higher primary beam intensities to reduce uncertainties (see text for details). (c) Profile of orthopyroxene. See Fig. 6 caption for description of uncertainties. Note the edges in these mineral fragments do not necessarily represent the true margins of the crystals.

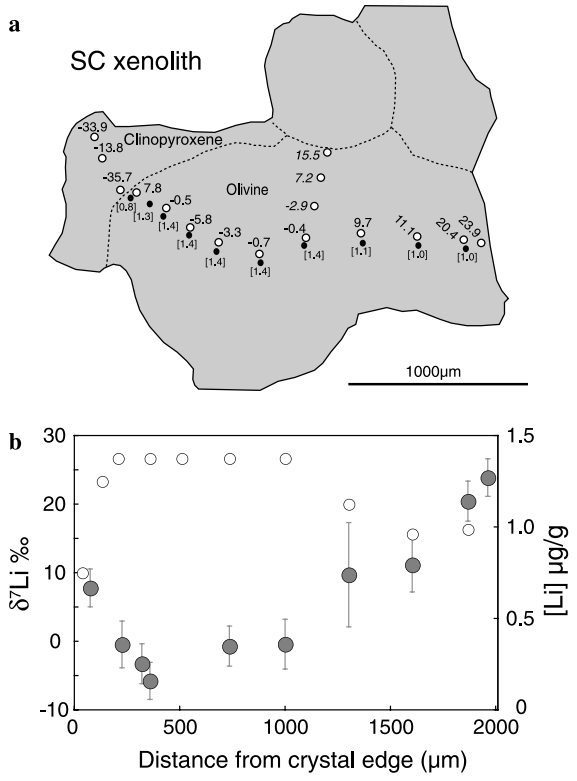

Fig. 9. (a) Trace outline of an olivine crystal from the SC xenolith olivine mounted in epoxy showing the position of the Li isotopic and Li concentration measurements (µg g^{-1}) by SIMS. (b) A corresponding plot of Li isotope (filled circles) and concentration (open circles) represented as a profile across the crystal. Points off the main line of the traverse are not plotted and shown on (a) in italics. See Fig. 6 caption for description of uncertainties.

values of δ^7Li up to 24‰ at the rim (Fig. 9b). The sense of elemental zoning of Li in the SC olivine (Fig. 9b) is also reversed compared to the olivines from the Vitim xenolith (Fig. 8a and b), with concentrations dropping from 1.3 µg g^{-1} in the core to 0.8 µg g^{-1} at the rim.

An isotope transect across a large (2 mm) orthopyroxene grain from the SC xenolith (Fig. 10a), shows a more complex zonation pattern (Fig. 10b). The rims yield δ^7Li ~ −5‰, the centre of the grain is anomalously light (δ^7Li −20 to −25‰) compared to bulk xenolith composition and there are significant troughs of δ^7Li −43‰ and −30‰ between the centre and the respective edges of the crystals. Again there is clear co-variation between Li concentration and δ^7Li in this grain (Fig. 10b). An adjacent ~800 µm clinopyroxene crystal shows a similar sense of isotopic zonation with edges (δ^7Li −4 to −8‰) heavier than an anomalously light core (δ^7Li −25 to −37‰), see Fig. 10c. In the clinopyroxene Li concentrations increase together with δ^7Li, unlike the inverse relationship seen in olivine (Fig. 9b) and the left-hand side of the large orthopyroxene (Fig. 10b) but reminiscent of the systematics of the right-hand side of the orthopyroxene in Fig. 10b.

All SIMS analyses of the single orthopyroxene shown in Fig. 10b are lighter than the MC-ICP-MS data on bulk orthopyroxene separates from SC (Table 3). We believe this reflects inter-grain δ^7Li variability in the SC sample, in addition to the extreme intra-grain variations clearly documented (Figs. 9 and 10), such that any individual crystal does not necessarily give a representative average for the bulk. Inter-grain heterogeneity is apparent in Fig. 10a, where a single analysis of a second, smaller orthopyroxene has a δ^7Li ~ 13‰, much heavier than any analysis of the adjacent grain we studied in detail.

5. Discussion

5.1. SIMS vs MC-ICP-MS measurements

Despite the absence of a matrix bias effect on SIMS Li isotope analyses for a wide range of mafic natural glass

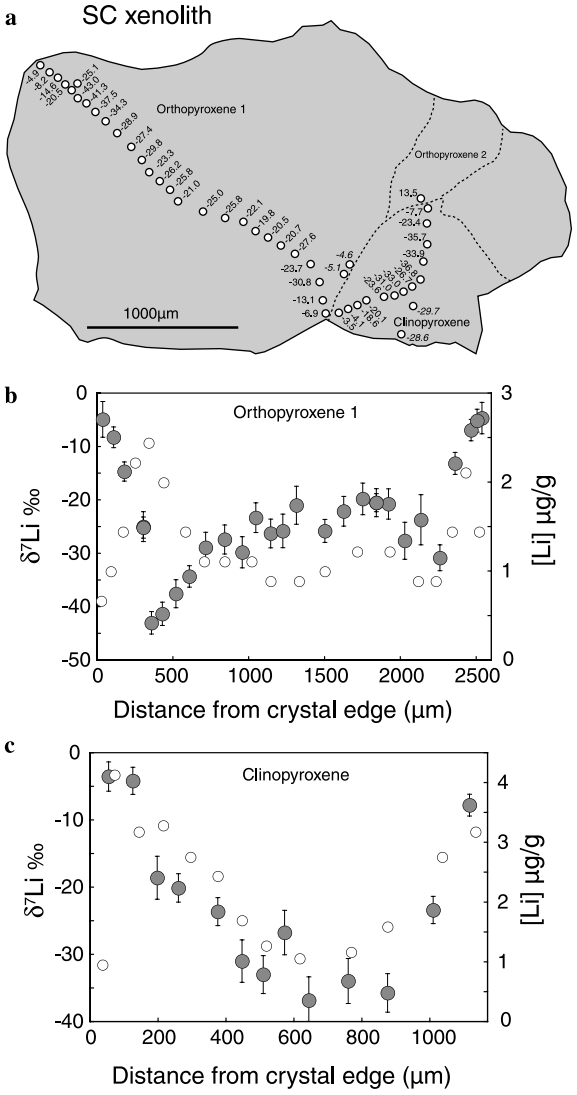

Fig. 10. (a) Trace outline of a crystal fragment of the SC xenolith showing the position of the Li isotopic and Li concentration measurements (µg g^{-1}) by SIMS on orthopyroxene and clinopyroxene crystals from the SC xenolith. Internal crystal boundaries are marked by dashed lines and the border with mounting epoxy is shown with a solid line. (b) and (c) are corresponding plots for orthopyroxene and clinopyroxene, respectively, of Li isotope (filled circles) and concentration (open circles) represented as profiles across the crystal. See Fig. 6 caption for description of uncertainties.

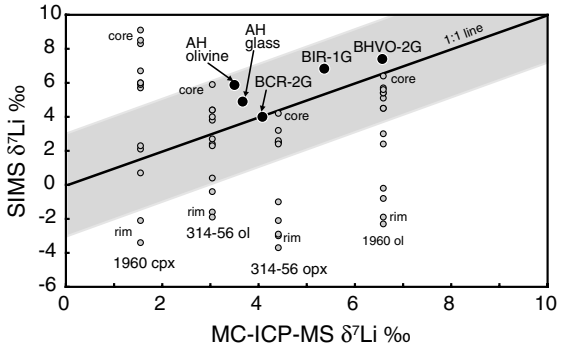

Fig. 11. Diagram showing the relationship between δ^7Li measurements by MC-ICP-MS and SIMS for a variety of minerals and glasses from this study, as well as some synthetic and natural glasses studied by Kasemann et al. (2005). The line represents a simple 1:1 reference line (not fitted to the standard data) and the shaded zone indicates a rough estimate of SIMS error of ±3‰ $2\sigma_{se}$. The analyses associated with rims and cores of individual the minerals are indicated. The SIMS measurements from this study are turned into δ^7Li values by using reference glass standard BCR-2G, which has a MC-ICP-MS value of 4.1‰, see Kasemann et al. (2005). The synthetic and natural glasses, including BCR-2G, BIR-1G and BHVO-2G measurements plotted, are taken from Kasemann et al. (2005), and these SIMS measurements were turned into δ^7Li values by referencing them to GSD-1G glass standard which has a MC-ICP-MS value of δ^7Li 31.14‰, see Kasemann et al. (2005). GSE-1G plots off scale but lies close to the 1:1 line with MC-ICP-MS value of δ^7Li 31.5, and a SIMS value of δ^7Li 32.0.

compositions (Kasemann et al., 2005), it is also important to assess the possible bias imparted by different mineral phases. Decitre et al. (2002) have previously reported no differential mass bias for SIMS Li isotope measurements between glass, olivine, clinopyroxene and orthopyroxene, which had been independently measured by TIMS. As discussed above, we have assumed this to be the case in conversion of our SIMS data to δ^7Li values. However, we wished to further explore this assumption using samples measured in this study.

Fig. 11 shows that the averaged, unzoned AH olivines formally plot within external reproducibility of the 1:1 correlation of SIMS and MC-ICP-MS measurements for USGS natural and synthetic reference materials (Kasemann et al., 2005). Nevertheless, the AH olivine average lies at the edge of this conservative error bound and notably yields a mean distinct from the standard error of AH glass run within the same analytical session (Fig. 4a and b). This suggests a significant (~2‰) instrumental mass bias in SIMS olivine analyses relative to basaltic glass.

Unfortunately, most other mineral phases we investigated by MC-ICP-MS turned out to be highly zoned when analysed by SIMS. It is thus difficult to compare bulk analyses by MC-ICP-MS and point analyses by SIMS. Calculating an average isotope composition of a three-dimensional crystal from a sparsely analysed, two-dimensional cross-section is challenging. Moreover, an unknown amount of the anomalously light rim is removed during crushing prior mineral separation for MC-ICP-MS. If the thin (~200–400 µm) isotopically perturbed rims are largely lost, this can help account for the reasonable agreement of MC-ICP-MS measurements with SIMS analyses of mineral cores (Fig. 11). Greater discrepancies between SIMS analyses of cores and bulk MC-ICP-MS analyses of the 1960 clinopyroxenes (Fig. 11) and the apparently unzoned 1955 plagioclase (Table 3 and EA-1) hint at differential mass bias between SIMS analyses of these phases and glass.

It is evident that our measurements of the zoned samples in this study are not ideal to assess robustly inter-mineral bias of δ^7Li by SIMS. In the absence of well-constrained data for all phases involved, we continue to follow the lead of Decitre et al. (2002) in not apportioning differential SIMS mass bias between mafic phases and glass, but note that this topic clearly requires further work. Since we are dominantly concerned in intra-mineral fractionations, the

inaccuracies of this approach do not influence our main conclusions. At worst, there is a 10‰ inaccuracy in assuming no differential instrumental mass bias between phases and in most cases it would appear to be considerably less (Fig. 11).

5.2. Melts and phenocrysts

The absence of significant Li isotope fractionation between olivine and melt in this study (Fig. 2a) is consistent with the observations made by Tomascak et al. (1999) and Chan and Frey (2003). Olivine fractionation or accumulation during magmatic differentiation thus should not perceptibly change the Li isotopic signature of the melt. Furthermore, as olivine is the dominant repository for Li in the mantle, Li isotopic fractionation during melting will also be limited (see Section 5.3.3).

An obvious complication to this simple picture lies in the zonation observed in the phenocrysts from 1960 Hawaiian flow (Fig. 6). This zonation is an inherent feature of pristine, phenocryst material and does not represent an alteration effect from Li isotope fractionation during adsorption onto secondary mineral (cf. Pistiner and Henderson, 2003). Such Li isotope variability within the crystals must arise from changing conditions during crystal grow or subsequent solid-state diffusion of Li. Significantly, Li has been shown to diffuse more rapidly than all other metal ions in melts (Richter et al., 2003) and plagioclase (Giletti and Shanahan, 1997). Diffusion coefficients of Li in clinopyroxene have also recently been determined and are found to range between 5×10^{-15} and 4×10^{-12} $m^2\,s^{-1}$ at temperatures of 800–1100 °C (Coogan et al., 2005). This predicts Li mobility in clinopyroxene several orders of magnitude faster than other common cations (e.g., Van Orman et al., 2001). Any isotopic disequilibrium must thus have been generated shortly before cooling of the magmas below a closure temperature for effective Li isotope exchange (~700 °C, Coogan et al., 2005). Although the high diffusivity of Li will ensure rapid isotopic equilibration at magmatic temperatures, equilibrium may be disturbed by continued diffusive movement of Li during cooling, at temperatures well below the point at which most cations are effectively immobile.

Qualitatively, an isotopically light rim can be caused by faster diffusion of ^{6}Li relative to ^{7}Li into a crystal. Diffusion of Li into phenocryst phases is also suggested by the higher concentrations of Li at their rims. This can in turn be explained as a natural consequence of cooling. Elemental mineral–melt partition coefficients increase with decreasing temperature, as long as the lattice strain energy of exchange is less than the free energy of mineral fusion, which is commonly the case (see Wood and Blundy, 1997). The latter is true for Li substitution into olivine and clinopyroxene and so the equilibrium concentration of Li in these phenocryst phases will increase with dropping temperature. As a lava cools, Li will diffuse into the phenocrysts, with ^{6}Li diffusing faster than ^{7}Li. This will lower the δ^7Li of the outer portion of the crystal, and also increase the concentration of lithium (Fig. 6). Faster isotopic self-diffusion relative to elemental diffusion can account for the narrower rims of elemental enrichment relative to isotope zonation, although the large errors in our individual isotope analyses make this hard to quantify definitively. The apparently broader zone of Li isotope and elemental zonation seen in the 97KC06 clinopyroxene relative to the olivine further suggests that Li diffusivity is greater in clinopyroxene.

The derivation of 97KC06 from magma mixing, as documented petrographically (Wright and Helz, 1996), provides clear support for the role of diffusion in generating zoned Li isotope profiles in minerals. The Li isotope zoning in the olivine and clinopyroxene of 97KC06 cannot simply result from mixing two magmas with different Li isotopic compositions. In major element terms, the 97KC06 olivine is normally and the clinopyroxene reversely zoned (Table 2) but both olivine and clinopyroxene have the same sense of Li isotope zoning. A mixing explanation for the Li isotope zonation would require the sense of core to rim Li isotope variation to be different in the olivine (derived from a more mafic magma) to that of the clinopyroxene (from a more evolved melt). Moreover, both olivine and clinopyroxene zone from cores with δ^7Li typical of Hawaiian whole rock analyses to isotopically anomalously rim compositions, lighter than any bulk Hawaiian lava analysis (Chan and Frey, 2003).

The absence of isotopic zoning in olivines in the glassy sample (AH, Fig. 4) provides additional support of a model involving diffusive fractionation of Li isotopes during lava cooling. Presumably the natural quenching of the AH samples gave insufficient time for a diffusive response to the increasing partition coefficient of Li in olivine, but maybe the extremely high diffusivity of Li in plagioclase (Giletti and Shanahan, 1997) resulted in some isotopic lightening of this phase despite the rapid cooling (Fig. 4c).

Bulk analyses of clinopyroxene and olivine separates by MC-ICP-MS represent averages of zoned crystals. Their measured compositions reflect the initial sizes of the crystals, their cooling rates and how much of the crystal rims was broken off during crushing and separation. Therefore, phenocryst phases are unlikely to provide robust measures of the original Li isotope ratios of holocrystalline lavas. This is unfortunate as picking fresh olivines from flows represents an attractive means of obtaining clearly unaltered material from older lavas for analysis (Chan and Frey, 2003). In some cases, MC-ICP-MS analyses of olivines and holocrystalline matrix do give the same δ^7Li (e.g., Th29) but this clearly cannot be assumed to be true in all situations and may simply be fortuitous.

5.3. Peridotite xenoliths

5.3.1. Bulk composition and inter-mineral fractionation

Olivine and to a lesser extent orthopyroxene dominate the Li budget of peridotites and thus their bulk Li isotope

compositions. Our MC-ICP-MS measurements of olivines and orthopyroxenes and reconstructed bulk compositions (Table 3 and Fig. 3c) overlap those of typical mantle-derived melts (Chan et al., 1992, 2002; Moriguti and Nakamura, 1998; Tomascak and Langmuir, 1999; Tomascak et al., 1999; Elliott et al., 2004; Ryan and Kyle, 2004). Our three most fertile, peridotites (313-102, 314-56 and MoZ-1) yield an average reconstructed bulk composition of $\delta^7Li = 3.6‰$. For reasons discussed below, we might wish to exclude the clinopyroxenes from the calculated bulk compositions but the modest modal abundances of clinopyroxene and its low Li concentrations make the average bulk composition insensitive (<0.1‰) to this detail. The value of $\delta^7Li \sim 3.5‰$ represents our best estimate for fertile CLM (i.e., relatively pristine peridotites, which experienced only minor, if any, melt extraction and metasomatism). The moderate depletions in light relative to heavy rare earth elements, together with MORB-like Sr–Nd–Hf–O isotope compositions of these xenoliths (Stosch et al., 1986; Ionov et al., 1994, 2005a,b; Ionov, 2004) suggest they may also be a good analogue for inferred mantle source of MORB. Notably, our reconstructed pristine xenoliths yield a δ^7Li that overlaps with recent high-precision measurements of normal, i.e., LREE-depleted, MORB (Elliott et al., 2004).

Given the limited range in olivine and orthopyroxene compositions in mantle xenoliths, the large variability of δ^7Li in clinopyroxenes is surprising. The isotopically heaviest clinopyroxene amongst our xenoliths (314-56), like the orthopyroxenes, is heavier than its co-existing olivine (Fig. 2). Three Central Asian samples studied by Magna et al. (2006) showed comparable systematics (Fig. 3a). This sense of isotopic fractionation is consistent with some studies of other 'light' elements in mantle minerals (Fig. 1). Hence, we suggest our heaviest Li isotope compositions in clinopyroxene are closest to isotopic equilibrium and that the lighter values are perturbed by late-stage diffusional processes, as discussed for our Hawaiian phenocrysts (see also Magna et al., 2006). Our phlogopite analysis displays an even more extreme light δ^7Li (−18.9‰), which we also attribute to effects of diffusive fractionation. The isotopic zonation observed in SIMS analyses of peridotite minerals (Figs. 8–10) further strongly point to recent diffusive processes influencing Li isotopic compositions.

The simplest patterns of Li isotope zonation are seen in olivine (Fig. 8a and b) and orthopyroxene (Fig. 8c) fragments from xenolith 314-56. The sense of isotopic and elemental variability is similar to that seen in phenocrysts of the 97KC06 Hawaii lava (Fig. 6), in that they show isotopically heavy cores with lower Li contents than the light rims. We again suggest that ^6Li preferentially diffuses into the xenoliths from the entraining magma or during related intrusive magmatism, shortly preceding transport of the mantle wall–rock fragment to the surface. This model implies melt pathways through the xenolith provide diffusionally fast access from magma to minerals in the interior of the nodule and that there is a chemical gradient that causes diffusion of Li from the melt into the xenolith.

Ionov (2004) noted that most of the Vitim xenoliths, including 314-56, locally contain veins and glass films around mineral phases, plausibly related to infiltration by the host melt or incipient melting of the nodules. Some San Carlos samples have also been shown to have interconnecting melt channels (Wirth, 1996). Our own SC sample is highly friable, suggesting melt has pervasively invaded between its minerals, allowing ready disaggregation. Thus melt networks through the xenoliths may connect minerals in the interior of the nodules to the reservoirs of Li in the entraining/intruding magmas. The latter are incompatible element-rich alkali magmas and likely contain Li concentrations in excess of that in equilibrium with the mineral phases in the xenolith, thereby driving a diffusional flux of Li into the minerals of the nodules.

Regardless of the ultimate causes of the chemical gradients, the Li concentration and isotopic profiles in mineral fragments shown in Fig. 8 strongly implicate a diffusive flux of Li into the crystals. Thus, the rims of the minerals in Fig. 8 are isotopically lighter than the unaffected cores which have δ^7Li close to the MC-ICP-MS analyses of bulk separates. This implies that the rims of olivine and orthopyroxene from 314-56 were largely abraded during preparation of bulk separates or discarded during hand-picking. Loss of isotopically light rims during sample preparation may also help account for the rather constant δ^7Li measured by MC-ICP-MS for olivine and orthopyroxene separates analysed for the other xenoliths. The Li isotope ratios of clinopyroxenes are more significantly perturbed and are evident in bulk MC-ICP-MS analyses even after possible loss of rim material during processing (Fig. 2). A combination of the following two factors may account for the greater influence of diffusion on the Li isotopic composition of clinopyroxene separates:

1. Clinopyroxene (and phlogopite) crystals are typically smaller than other minerals, especially in more depleted nodules with lower modal abundance. Hence a smaller proportion of pristine clinopyroxene core is preserved for a given diffusion time compared to olivine and orthopyroxene.
2. Observations from the Hawaiian phenocrysts suggest higher diffusivity of Li in clinopyroxene relative to olivine.

The isotopic zoning observed in mineral fragments in the refractory peridotite SC analysed by SIMS is more complex than in the fertile Vitim xenolith 314-56. To account for the extreme Li isotopic compositions in some of the SC minerals (δ^7Li −40‰) we invoke a two-stage diffusive process. We suggest ^6Li preferentially diffuses through interstitial melt veins before further isotopic fractionation occurs during solid-state diffusion into minerals. An isotopically light interstitial melt film that pervades some xenoliths can also explain why the measured δ^7Li in

the bulk San Carlos xenolith of Seitz et al. (2004) is ~2.5‰ lighter than the reconstructed bulk Li isotopic composition from individually measured minerals of the same sample (Fig. 3c). Given that the proportion of incipient or infiltrated melt in this xenolith is very small (<0.1%) this implies an extremely low δ^7Li for the melt. As discussed by Lundstrom et al. (2005) differential diffusion of Li isotopes within the melt phase alone can readily explain isotopic compositions of $\delta^7\text{Li} \sim -20‰$ in melts invading peridotite. Time dependent evolution of the Li isotopic composition interstitial melts can potentially result in the reversed sense of Li isotope zonation observed in the SC xenolith (Figs. 9 and 10) relative to the Hawaiian phenocrysts and the W profiles seen in the orthopyroxene (Fg. 10b).

Detailed modelling of the mineral profiles is beyond the scope of this paper but in general terms it is clear from the high diffusivity of Li (Coogan et al., 2005) that any Li isotope heterogeneity on a mineral scale must have been imparted shortly (less than a few years) before cooling. This suggests isotopic disequilibrium was created during the episode of magmatism that ultimately brought the xenolith to the surface, if not the process of entrainment and final cooling itself. The *in situ* Li isotope analyses therefore provide strong evidence that the isotopically light clinopyroxene (and phlogopite) compositions result from 'late-stage' effects and do not represent widespread mantle compositions.

Given the zoned isotopic profiles of all the peridotite minerals we examined (albeit of limited total number), we need to interpret bulk separate δ^7Li data with caution. As discussed above, however, good agreement between δ^7Li of olivine and orthopyroxene cores of samples 314-56 measured by SIMS and bulk separates determined by MC-ICP-MS suggests that our preparation process fortuitously removed the isotopically anomalous rims of these two major phases or that zoning is not as common as implied by our initial study. The MC-ICP-MS data on the four spinel peridotite samples for which we have olivine and orthopyroxene analyses indicate a rather constant fractionation between these two phases (Table 3 and Fig. 2b). This may plausibly be interpreted as high-temperature equilibrium fractionation, yielding $\alpha_{\text{ol-opx}}$ of 0.9985 ($\pm$0.0003, $2\sigma_{\text{sd}}$).

5.3.2. Comparison with other studies

Seitz et al. (2004) published a major MC-ICP-MS δ^7Li study on bulk separates from peridotite nodules. Although the δ^7Li of our olivines (and hence bulk perdotite compositions) show a similar range to the olivines from the unmetasomatised peridotites of Seitz et al. (2004), see Fig. 3c, the sense of inter-mineral isotopic fractionation in our two studies is very different. Seitz et al. (2004) found that the δ^7Li of the main minerals decreased systematically in the order olivine > orthopyroxene > clinopyroxene. The authors also inferred diminishing isotopic fractionation between olivine and clinopyroxene with increasing equilibrium temperature. In contrast, the peridotite mineral analyses in more recent study of Magna et al. (2006) are in good agreement with our findings.

The reasons for the differences between our study and that of Seitz et al. (2004) are not clear and further work is required to resolve these issues. We can speculate, however, that the xenoliths analysed by Seitz et al. (2004) may contain pyroxenes more influenced by the process of diffusive decrease in δ^7Li described above. Strikingly, Seitz et al. (2004) stressed the importance of ultra-sonic cleaning, noting that δ^7Li measurements made without this treatment were lower. We suggest that this ultra-sounic cleaning removed additional portions of isotopically light rims and/or adhering interstitial glass. Seitz et al. (2004) may thus have been analysing samples containing largely intact rims. We believe that the vigorous ultra-sonic treatment our separates received during mineral separation (Section 3.1) had already dominantly ablated most of our mineral rims. This made our measurement procedure insensitive to additional ultra-sound treatment (Section 3.1 and Table 3) and resulted in our MC-ICP-MS measurements yielding δ^7Li values closer to core compositions, especially for the strongly diffusionally influenced clinopyroxenes. Notably Magna et al. (2006) analysed peridotites from the same Central Asian collection that we studied, and their separates had undergone the same ultra-sonic pre-treatment. It is also worth adding that we analysed a greater number of fertile samples than Seitz et al. (2004), in which the large clinopyroxenes are likely to be less diffusionally perturbed than in clinopyroxene poor, depleted samples (Fig. 3a).

A study of nodules from Far East Russian and SW Japanese localities by Nishio et al. (2004) reported clinopyroxenes with δ^7Li as low as $-17‰$, a value comparable to that of our metasomatic phlogopite. Nishio et al. (2004) did not present associated olivine or orthopyroxene analyses, focussing only on clinopyroxene as the major host of the traditional radiogenic isotope tracers Sr and Nd. The authors inferred a deep recycled origin of the light δ^7Li, noting that the only other comparably light Li isotopic analyses then measured were in eclogites inferred to be dehydrated, subducted oceanic crust (Zack et al., 2003). Seitz et al. (2004) pointed out that Nishio et al.'s (2004) anomalously light clinopyroxenes also had elevated Li abundances and this leads to a broad negative correlation of δ^7Li with lithium concentration (not shown). We suggest that these features may be explained as the result of diffusional processes during entrainment, even more extreme than those observed in our SC sample (Fig. 10c). Additional *in situ* analyses of the clinopyroxenes and co-existing phases would be necessary to substantiate this suggestion.

Finally, we highlight that the style of Li isotope zoning observed in the SIMS profile of our SC clinopyroxene is reminiscent of the isotopic profile of a clinopyroxene in Martian meteorite, NWA 480 reported by Beck et al. (2004). This pyroxene shows isotope zonation from $\delta^7\text{Li} \sim -17‰$ in the core up to $+10‰$ at the rim. To explain this observation, Beck et al. (2004) inferred a Rayleigh fractionation of Li during water loss from a

co-existing melt during its crystallisation. We have illustrated that extreme isotope zonation of Li may occur through normal magmatic processes on Earth, and so, the magnitude and style of the Li isotopic fractionation observed in SNC meteorite NWA 480 is not necessarily related to processes specific to Mars.

5.3.3. Further ramifications

A primary goal of this study was to assess possible equilibrium fractionation of Li isotopes during mantle melting. To this end, we assume that our olivine-orthopyroxene fractionation of 0.9985 in the spinel perditotes is an equilibrium effect and couple this with our observation of negligible olivine–melt fractionation derived from olivine–melt pairs. We additionally assume olivine-clinopyroxene fractionation equal to olivine-orthopyroxene and ignore the influence of garnet and spinel, which little influence the overall calculation due to their low Li contents. Fig. 12 shows the results of this calculation for the δ^7Li of melt after different degrees of melting. Since the Li budget is most strongly influenced by olivine–melt equilibrium, fractionation of the Li isotope ratio of a melt relative to its source is small (<0.5‰) and rather constant (±0.15‰) over representative degrees of mantle melting. The calculation likely over-estimates fractionation by using inferred fractionation factors between olivine and orthopyroxene for xenoliths with equilibration temperatures (~900–1100 °C, see Table 2) lower than typical melting temperatures (~1200 °C). The Li isotopic composition of mantle-derived melts should provide a good estimate of their source, albeit ~0.2–0.5‰ too light.

Nevertheless, a corollary of the record of diffusive fractionation observed in peridotites is that erupted melts may also have their Li isotopic composition changed by non-equilibrium effects. A full assessment of this possibility requires a detailed modelling effort beyond the scope of this manuscript. The recent study by Lundstrom et al. (2005) clearly identifies the role of diffusive fractionation of Li in mantle processes and allows an estimate of its effect on the δ^7Li of erupted melts to be made. Lundstrom et al. (2005) report SIMS transects which show 'troughs' of low δ^7Li in the olivines of peridotite adjacent to dunite dykes. The dykes are interpreted as palaeo-melt channels (cf. Kelemen et al., 1995), and Lundstrom et al. (2005) develop a quantitative model of preferential, diffusive ^{6}Li transport out of the melt channels into the surrounding perditotite to account for their observations.

We have calculated a net flux of ^{6}Li from melt conduit to surrounding mantle required to generate the δ^7Li profile TP90-9 from the Josephine peridotite (Lundstrom et al., 2005). We assume all melt conduits have comparable isotopic profiles and that all melt leaves the sub-ridge melting domain via such conduits. A critical parameter is the spacing between the conduits, which in our simple mass

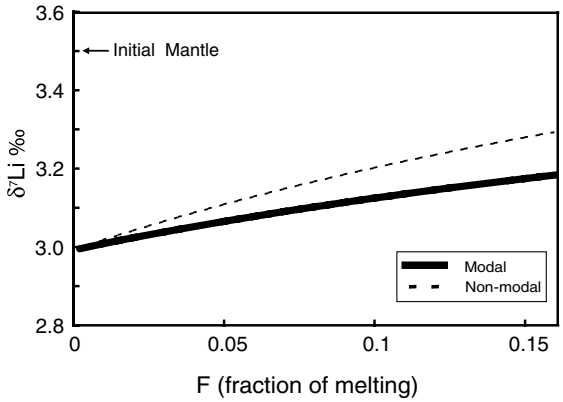

Fig. 12. Calculated δ^7Li of a melt in equilibrium with a source (initial δ^7Li = 3.5‰) at different degrees of melting (by mass). Modal (black line) and non-modal (dashed line) melting scenarios are illustrated. As inferred from our data (Fig. 2) we assume no isotopic fractionation between olivine and melt, $\alpha_{ol\text{-}opx}$ and the same fractionation for clinopyroxene as orthopyroxene. We ignore the influence of the low Li concentration aluminous phase. The modal composition of the mantle is assumed to be 60% olivine, 25% orthopyroxene, and 15% clinopyroxene. Non-modal melting modes are Ol = −0.1, Opx = 0.3, Cpx = 0.8. Partion coefficients used for Li are $D^{Li}_{Ol} = 0.35$, $D^{Li}_{Opx} = D^{Li}_{Cpx} = 0.27$ (after Brenan et al., 1998).

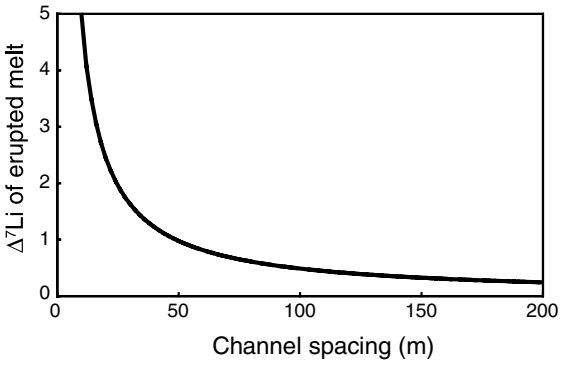

Fig. 13. Change in the δ^7Li of a melt (expressed as a difference from primary composition) as a result of diffusive fractionation in the melt conduit. The change in lithium isotope composition (Δ^7Li) is plotted as a function of the spacing of the melt channels. This simplistic calculation is made assuming a net flux of ^{6}Li from melt conduit to surrounding mantle, determined from a graphical integration of the δ^7Li profile of TP90-9 from the Josephine peridotite (Lundstrom et al., 2005). Given a similar profile on each side of every conduit, this requires a net addition of 7.4×10^{-4} mol ^{6}Li from melt channel to country rock. We assume that the dunite channel in the Josephine peridotite represents the top of a steady-state melt conduit, through which all melt generated below must pass before eruption. The flux of melt that passes through a conduit (with regular spacing x metres) for mantle (density ρ_m) with an upwelling velocity of u is $x \cdot \rho_m \cdot F \cdot u$, where F is the degree of melting (expressed as a conventional weight fraction). From this melt flux there is a net loss of $u \cdot 7.4 \times 10^{-4}$ ^{6}Li to the country rock. The ^{7}Li/^{6}Li of the erupted melt can thus be calculated as $[u \cdot x \cdot \rho_m \cdot F \cdot [\mathrm{Li}] \cdot 10^{-6}/(6.02/^7\mathrm{Li}/^6\mathrm{Li} + 7.02)]/[u \cdot x \cdot \rho_m \cdot F \cdot [\mathrm{Li}] \cdot 10^{-6}/(6.02 + 7.02 \cdot {}^7\mathrm{Li}/{}^6\mathrm{Li}) - u \cdot 7.4 \times 10^{-4}]$, where ^{7}Li/^{6}Li is the (atomic) Li isotope ratio and [Li] the elemental concentration of Li (in μg g^{-1}) in the primary melt and the constants 6.02 and 7.02 are the relative nuclide masses of ^{6}Li and ^{7}Li. The values plotted in the figure are calculated relative to an initial ^{7}Li/^{6}Li value of 12.231, i.e., δ^7Li = 5‰, the background mantle value in the Lundstrom et al. (2005) study, using [Li] = 5 μg g^{-1}, $\rho_m = 3.3 \times 10^6$g m^{-3} and $F = 0.1$ for varying channel spacing. If such melt conduits are spaced at intervals >50 m the influence of diffusive loss is <1‰ on the δ^7Li of the erupted melt and <0.5‰ if the conduit spacing is >100 m.

balance, scales with how much melt is delivered via a single melt channel. The more melt passed through a single channel, the smaller the influence of the given ^{6}Li flux to the surrounding mantle on the integrated Li isotope composition of the melt transferred to the surface. If melt conduits are spaced at intervals greater than 50 m (Fig. 13), the influence of diffusive loss of Li to the peridotite is <1‰. This exercise requires a more extensive study of different thickness dykes to relate to their power-law distribution in ophiolites (Braun and Kelemen, 2002). Interestingly, equilibrium fractionation during melting and diffusive fractionation act in different directions, and the net effect of both processes may be to leave the δ^7Li of the melt insignificantly changed with respect to its source.

The rapid diffusive response of Li isotopes to pre-eruptive events could provide a very sensitive chronometer of these processes. For example, the cooling rate of lavas could be assessed by the degree of Li isotope zoning in large mineral grains. In contrast to the elemental geospeedometers (Berlo et al., 2004; Costa and Chakraborty, 2004), Li isotopic zonation has the advantage that it should respond dominantly to diffusional processes during cooling rather than changes in equilibrium during late-stage crystal growth. This is an exciting potential field to explore.

6. Conclusions

Unmetasomatised, fertile peridotite xenoliths from the CLM have a bulk δ^7Li ~ 3.5‰. Although fertile in major element terms, these samples are incompatible element depleted, like the MORB source, and so provide a reasonable estimate for the δ^7Li of typical upper mantle. Measurements of co-existing olivine-glass pairs show negligible Li isotope olivine–melt fractionation, whereas mineral separate analyses from spinel peridotites suggest that orthopyroxenes have apparent equilibrium values ~1.5‰ heavier than olivines. Olivine and to a lesser extent orthopyroxene dominate the Li budget of the mantle and its partitioning into melt. Our measurements thus enable us to calculate the magnitude of Li isotope fractionation during mantle melting. Melts are <0.2–0.5‰ lighter than their mantle sources and this fractionation is relatively insensitive to variable degrees of melting or modest changes in mineralogy. During migration to the surface, the Li isotope ratios of melts may be modified as a result of diffusive loss of ^{6}Li to wall–rock peridotite (Lundstrom et al., 2005). The magnitude of this effect is not well known, but we show that it is plausibly small (<1‰). Therefore, it is likely that analysis of primitive mantle melts should provide a good approximation (better than 0.5‰) of the δ^7Li of their sources.

SIMS isotopic profiles of olivine and pyroxenes in mantle xenoliths reveal Li isotopic zonation. These features reflect isotopic disequilibrium that must have been imparted only few years before cooling of the xenolith at the surface. Similar isotopic zoning is also observed in Hawaiian phenocrysts in holocrystalline (but not glassy) samples, suggesting isotopic re-distribution occurred during cooling of the lava flows. The most common Li isotope profiles in minerals, with rims having lighter δ^7Li and higher Li concentrations than the cores, may be best explained by more rapid diffusion of ^{6}Li into the mineral grains. More complex zoning patterns seen in some xenolith minerals may result from two stages of isotopic fractionation. The Li isotope compositions of clinopyroxene in mantle xenoliths are much more variable than those for olivine or orthopyroxene and include δ^7Li values as light as −8‰ in bulk clinopyroxene separates. A single phlogopite analysis yielded δ^7Li = −18.9‰. These observations suggest more extensive ingress of ^{6}Li into clinopyroxene and phlogopite as a result of faster diffusion and their typically smaller grain sizes.

Diffusive fractionation appears to be an important process in influencing high-temperature distribution of Li isotopes and is evident in results of other studies (Richter et al., 2003; Lundstrom et al., 2005; Teng et al., 2006). The high diffusivity of Li means that measurements of Li isotope zoning, which appears to be common in igneous minerals, have potential as a high-resolution geospeedometer.

Acknowledgments

We are grateful to Chris Coath (University of Bristol) for help with MC-ICP-MS, Stuart Kearns (University of Bristol) for help with electron micro-probe, Nicola Cayzer (University of Edinburgh) for help with the scanning electron microscope and Dave Bromiley and John Wade (University of Bristol) for help with micro-analytical sample preparation. We are grateful for the reviews of Paul Tomascak, Ivan Vlastélic and an anonymous reviewer and we have hopefully tightened up our arguments as a result of their efforts. Thanks are also due to Julie Prytulak for her helpful comments. This work was part of a NERC studentship NER/S/A/2001/06000, supplemented with grants to use the Edinburgh ion-probe facility (IMP215/1003 and IMP240/1004) and further supported by a Sir Philip Leverhulme Prize awarded to TE.

Associate editor: Martin A. Menzies

Appendix A. Supplementary data

Supplementary data associated with this article can be found, in the online version, at doi:10.1016/j.gca.2006.06.1611.

References

Beard, B.L., Johnson, C.M., 2004. Inter-mineral Fe isotope variations in mantle-derived rocks and implications for the Fe geochemical cycle. *Geochim. Cosmochim. Acta* **68**, 4727–4743.

Beck, P., Barrat, J.A., Chaussidon, M., Gillet, P., Bohn, M., 2004. Li isotopic variations in single pyroxenes from the Northwest Africa 480 shergottite (NWA 480): a record of degassing of Martian magmas? *Geochim. Cosmochim. Acta* **68**, 2925–2933.

Berlo, K., Blundy, J., Turner, S.P., Kashman, K., Hawkesworth, C.J., Black, S., 2004. Geochemical precursors to volcanic activity at Mount St. Helens, USA. *Science* **306**, 1167–1169.

Braun, M.G., Kelemen, P.B., 2002. Dunite distribution in the Oman ophiolite: implications for melt flux through porous dunite conduits. *Geochem. Geophys. Geosyst.* **3**, 8603. doi:10.1029/2001GC000289.

Brenan, J.M., Neroda, E., Lundstrom, C.C., Shaw, H.F., Ryerson, F.J., Phinney, D.L., 1998. Behaviour of boron, beryllium and lithium during melting and crystallisation: constraints from mineral–melt partitioning experiments. *Geochim. Cosmochim. Acta* **62**, 2129–2141.

Chan, L.H., Edmond, J.M., Thompson, G., Gillis, K., 1992. Lithium isotopic composition of submarine basalts: implications for the lithium cycle in the oceans. *Earth Planet. Sci. Lett.* **108**, 151–160.

Chan, L.H., Frey, F.A., 2003. Lithium isotope geochemistry of the Hawaiian plume: results from the Hawaii Scientific Drilling Project and Koolau volcano. *Geochem. Geophys. Geosyst.* **4**, 8707. doi:10.1029/2002GC000365.

Chan, L.H., Leeman, W.P., You, C.F., 2002. Lithium isotopic composition of Central American volcanic arc lavas: implications for modification of subarc mantle by slab-derived fluids: correction. *Chem. Geol.* **182**, 293–300.

Chazot, G., Lowry, D., Menzies, M., Mattey, D., 1997. Oxygen isotopic composition of hydrous and anhydrous mantle peridotites. *Geochim. Cosmochim. Acta* **61**, 161–169.

Coogan, L.A., Kasemann, S.A., Chakraborty, S., 2005. Rates of hydrothermal cooling of new oceanic upper crust derived from lithium-geospeedometry. *Earth Planet. Sci. Lett.* **240**, 415–424.

Cooper, K.M., Reid, M.R., Murrell, M.T., Clague, D., 2001. Crystal and magma residence at Kilauea volcano, Hawaii: ^{230}Th-^{226}Ra dating of the 1955 east rift eruption. *Earth Planet. Sci. Lett.* **184**, 703–718.

Costa, F., Chakraborty, S., 2004. Decadal time gaps between mafic intrusion and silicic eruption obtained from chemical zoning patterns in olivine. *Earth Planet. Sci. Lett.* **227**, 517–530.

Decitre, S., Deloule, E., Reisberg, L., James, R., Agrinier, P., Mével, C., 2002. Behavior of Li and its isotopes during serpentinization of oceanic peridotites. *Geochem. Geophys. Geosyst.* **3**, 1007. doi:10.1029/2001GC000178.

Elliott, T., Hawkesworth, C., Grönvold, K., 1991. Dynamic melting of the Iceland plume. *Nature* **351**, 201–206.

Elliott, T., Jeffcoate, A.B., Bouman, C., 2004. The terrestrial Li isotope cycle: light-weight constraints on mantle convection. *Earth Planet. Sci. Lett.* **220**, 231–245.

Frey, F.A., Prinz, M., 1978. Ultramafic inclusions from San Carlos, Arizona: petrological and geochemical data bearing on their petrogenesis. *Earth Planet. Sci. Lett.* **38**, 129–176.

Galer, S.J.G., O'Nions, R.K., 1998. Chemical and isotopic studies of ultramafic inclusions from San Carlos volcanic field, Arizona: a bearing on their petrogenesis. *J. Petrol.* **30**, 1033–1064.

Giletti, B.J., Shanahan, T.M., 1997. Alkali diffusion in plagioclase feldspar. *Chem. Geol.* **139**, 3–20.

Heliker, C., Mangan, M.T., Mattox, T.N., 1998. The character of long-term eruptions: inferences from episodes 50–53 of the Pu'u 'O'o-Kupaianaha eruption of Kilauea Volcano. *Bull. Volcanol.* **59**, 381–393.

Hirose, K., Kushiro, I., 1993. Partial melting of dry peridotites at high-pressures: determination of compositions of melts segregated from peridotite using aggregates of diamond. *Earth Planet. Sci. Lett.* **114**, 477–489.

Huh, Y., Chan, L.H., Edmond, J.M., 2001. Lithium isotopes as a probe of weathering processes: Orinoco River. *Earth Planet. Sci. Lett.* **194**, 189–199.

Ionov, D., 2004. Chemical variations in peridotite xenoliths from Vitim, Siberia: inferences for REE and Hf behaviour in the garnet-facies upper mantle. *J. Petrol.* **45**, 343–367.

Ionov, D.A., Ashchepkov, I.V., Jagoutz, E., 2005a. The provenance of fertile off-craton lithospheric mantle: Sr–Nd isotope and chemical composition of garnet and spinel peridotite xenoliths from Vitim, Siberia. *Chem. Geol.* **217**, 41–75.

Ionov, D.A., Blichert-Toft, J., Weis, D., 2005b. Hf isotopic compositions and HREE variations in off-craton spinel peridotite xenoliths from central Asia. *Geochim. Cosmochim. Acta* **69**, 2399–2418.

Ionov, D.A., Ashchepkov, I.V., Stosch, H.G., Witteickschen, G., Seck, H.A., 1993. Garnet peridotite xenoliths from the Vitim volcanic field, Baikal region: the nature of the garnet-spinel peridotite transition zone in the continental mantle. *J. Petrol.* **34**, 1141–1175.

Ionov, D.A., Harmon, R.S., France-Lanord, C., Greenwood, P.B., Ashchepkov, I.V., 1994. Oxygen-isotope composition of garnet and spinel peridotites in the continental mantle: evidence from the Vitim xenolith suite, southern Siberia. *Geochim. Cosmochim. Acta* **58**, 1463–1470.

Ionov, D.A., Wood, B.J., 1992. The oxidation state of subcontinental mantle: oxygen thermobarometry of mantle xenoliths from central Asia. *Contrib. Mineral. Petrol.* **111**, 179–193.

Jeffcoate, A.B., Elliott, T., Thomas, A., Bouman, C., 2004. Precise, small sample size determination of lithium isotopic compositions of geological reference materials and modern seawater by MC-ICP-MS. *Geostand. Geoanal. Res.* **28**, 161–172.

Kasemann, S.A., Jeffcoate, A.B., Elliott, T., 2005. Lithium isotope composition of basalt glass reference material. *Anal. Chem.* **77**, 5251–5257.

Kelemen, P.B., Shimizu, N., Salters, V.J.M., 1995. Extraction of mid-ocean-ridge basalt from the upwelling mantle by focused flow of melt in dunite channels. *Nature* **375**, 747–753.

Kyser, T.K., 1986. Stable isotope variations in the mantle. In: Valley, J.W., Taylor, H.P., O'Neill, J.R. (Eds.), *Stable Isotopes in High Temperature Geological Processes*. Mineralogical Society of America, Washington, DC, pp. 41–162.

Lundstrom, C.C., Chaussidon, M., Hsui, A.T., Kelemen, P., Zimmerman, M., 2005. Observations of Li isotopic variations in the Trinity Ophiolite: evidence for isotopic fractionation by diffusion during mantle melting. *Geochim. Cosmochim. Acta* **69**, 735–751.

Magna, T., Wiechert, U., Halliday, A.N., 2006. New constraints on the lithium isotope compositions of the Moon and terrestrial planets. *Earth Planet. Sci. Lett.* **243**, 336–353.

Mattey, D., Lowry, D., Macpherson, C., 1994. Oxygen-isotope composition of mantle peridotite. *Earth Planet. Sci. Lett.* **128**, 231–241.

Moriguti, T., Nakamura, E., 1998. Across-arc variation of Li isotopes in lavas and implications for crust/mantle recycling at subduction zones. *Earth Planet. Sci. Lett.* **163**, 167–174.

Nishio, Y., Nakai, S., Yamamoto, J., Sumino, H., Matsumoto, T., Prikhod'ko, V.S., Arai, S., 2004. Lithium isotopic systematics of the mantle-derived ultramafic xenoliths: implications for EM1 origin. *Earth Planet. Sci. Lett.* **217**, 245–261.

Pearce, N.J.G., Perkins, W.T., Westgate, J.A., Gorton, M.P., Jackson, S.E., Neal, C.R., Chenery, S.P., 1997. A compilation of new and published major and trace element data for NIST SRM 610 and NIST SRM 612 glass reference materials. *Geostandard Newslett.* **21**, 115–144.

Pistiner, J.S., Henderson, G.M., 2003. Lithium-isotope fractionation during continental weathering processes. *Earth Planet. Sci. Lett.* **214**, 1–13.

Press, S., Witt, G., Seck, H.A., Ionov, D., Kovalenko, V.I., 1986. Spinel peridotite xenoliths from the Tariat Depression, Mongolia. I. Major element chemistry and mineralogy of a primitive mantle xenolith suite. *Geochim. Cosmochim. Acta* **50**, 2587–2599.

Richter, F.M., Davis, A.M., DePaolo, D.J., Watson, E.B., 2003. Isotope fractionation by chemical diffusion between molten basalt and rhyolite. *Geochim. Cosmochim. Acta* **67**, 3905–3923.

Ryan, J.G., Kyle, R.P., 2004. Lithium abundance and lithium isotope variations in mantle sources: insights from intraplate volcanics from Ross Island and Marie Byrd Land (Antartica) and other oceanic islands. *Chem. Geol.* **212**, 125–142.

Seitz, H.M., Brey, G.P., Lahaye, Y., Durali, S., Weyer, S., 2004. Lithium isotopic signatures of peridotite xenoliths and isotopic fractionation at high temperature between olivine and pyroxenes. *Chem. Geol.* **212**, 163–177.

Seitz, H.M., Woodland, A.B., 2000. The distribution of lithium in peridotitic and pyroxenitic mantle lithologies: an indicator of magmatic and metasomatic processes. *Chem. Geol.* **166**, 47–64.

Stosch, H.G., Lugmair, G.W., Kovalenko, V.I., 1986. Spinel peridotite xenoliths from the Tariat Depression, Mongolia. II: geochemistry and Nd and Sr isotopic composition and their implications for the evolution of the subcontinental lithosphere. *Geochim. Cosmochim. Acta* **50**, 2601–5614.

Teng, F.Z., McDonough, W.F., Rudnick, R.L., Walker, R.J., 2006. Diffusion-driven extreme lithium isotopic fractionation in country rocks of the Tin Mountain pegmatite. *Earth Planet. Sci. Lett.* **243**, 701–710.

Tomascak, P.B., 2004. Developments in the understanding and application of lithium isotopes in the Earth and planetary sciences. In: Johnson, C.M., Beard, B.L., Albarède, F. (Eds.), *Geochemistry of Non-traditional Stable Isotopes*. Mineralogical Society of America, Washington, DC, pp. 153–195.

Tomascak, P.B., Langmuir, C.H., 1999. Lithium isotope variability in MORB. *EOS Trans. AGU* **80**, 10–V11E.

Tomascak, P.B., Tera, F., Helz, R.T., Walker, R.J., 1999. The absence of lithium isotope fractionation during basalt differentiation: new measurements by multicollector sector ICP- MS. *Geochim. Cosmochim. Acta* **63**, 907–910.

Van Orman, J.A., Grove, T.L., Shimizu, N., 2001. Rare earth element diffusion in diopside: influence of temperature, pressure, and ionic radius, and an elastic model for diffusion in silicates. *Contrib. Mineral. Petrol.* **141**, 687–703.

Williams, H.M., Peslier, A.H., McCammon, C., Halliday, A.N., Levasseur, S., Teutsch, N., Burg, J.-P., 2005. Systematic iron isotope variations in mantle rocks and minerals: the effects of partial melting and oxygen fugacity. *Earth Planet. Sci. Lett.* **235**, 435–452.

Wood, B.J., Blundy, J.D., 1997. A predictive model for rare earth element partitioning between clinopyroxene and anhydrous silicate melt. *Contrib. Mineral. Petrol.* **129**, 166–181.

Wirth, R., 1996. Thin amorphous films (1–2 nm) at olivine grain boundaries in mantle xenoliths from San Carlos, Arizona. *Contrib. Mineral. Petrol.* **124**, 44–54.

Wright, T.L., Fiske, R.S., 1971. Origin of the differentiated and hybrid lavas of Kilaeua volcano, Hawaii. *J. Petrol.* **12**, 1–65.

Wright, T.L., Helz, R.T., 1996. Differentiation and magma mixing on Kilaeua's east rift zone: a further look at the eruptions of 1955 and 1960. 2. The 1960 lavas. *Bull. Volcanol.* **57**, 602–630.

Young, E.D., Ash, R.D., Galy, A., Belshaw, N.S., 2002. Mg isotope heterogeneity in the Allende meteorite measured by UV laser ablation-MC-ICP-MS and comparisons with O isotopes. *Geochim. Cosmochim. Acta* **66**, 683–698.

Zack, T., Tomascak, P.B., Rudnick, R.L., Dalpé, C., McDonough, W.F., 2003. Extremely light Li in orogenic eclogites: the role of isotope fractionation during dehydration in subducted oceanic crust. *Earth Planet. Sci. Lett.* **208**, 279–290.

Zhang, L.B., Chan, L.H., Gieskes, J.M., 1998. Lithium isotope geochemistry of pore waters from Ocean Drilling Program Sites 918 and 919, Irminger Basin. *Geochim. Cosmochim. Acta* **62**, 2437–2450.

Zhu, X.K., Guo, Y., Williams, R.J.P., O'Nions, R.K., Matthews, A., Belshaw, N.S., Canters, G.W., de Waal, E.C., Weser, U., Burgess, B.K., Salvato, B., 2002. Mass fractionation processes of transition metal isotopes. *Earth Planet. Sci. Lett.* **200**, 47–62.

Zindler, A., Jagoutz, E., 1988. Mantle cryptology. *Geochim. Cosmochim. Acta* **52**, 319–333.